CHEMISTRY

Calcium-looping reforming of methane realizes in situ CO_2 utilization with improved energy efficiency

Sicong Tian[1]*, Feng Yan[2,3], Zuotai Zhang[2], Jianguo Jiang[3]

Closing the anthropogenic carbon cycle is one important strategy to combat climate change, and requires the chemistry to effectively combine CO_2 capture with its conversion. Here, we propose a novel in situ CO_2 utilization concept, calcium-looping reforming of methane, to realize the capture and conversion of CO_2 in one integrated chemical process. This process couples the calcium-looping CO_2 capture and the CH_4 dry reforming reactions in the CaO-Ni bifunctional sorbent-catalyst, where the CO_2 captured by CaO is reduced in situ by CH_4 to CO, a reaction catalyzed by catalyzed by the adjacent metallic Ni. The process coupling scheme exhibits excellent decarbonation kinetics by exploiting Le Chatelier's principle to shift reaction equilibrium through continuous conversion of CO_2, and results in an energy consumption 22% lower than that of conventional CH_4 dry reforming for CO_2 utilization. The proposed CO_2 utilization concept offers a promising option to recycle carbon directly at large CO_2 stationary sources in an energy-efficient manner.

INTRODUCTION

Carbon capture and storage (CCS), renewable energy development, and end-use energy efficiency improvement are the three main strategies to limit global warming to well below 2°C, as pledged in the Paris Agreement, and are projected to contribute about 82% of cumulative reductions in global CO_2 emissions up to 2050 (*1*, *2*). Among these strategies, CCS is a major low-carbon option applicable to large stationary sources of CO_2, including coal-fired power plants and energy-intensive industrial sectors (*3*). With regard to the current development of the CCS strategy, interest is increasing in using the CO_2 captured from fossil fuel combustion and industrial processes as a feedstock for chemical production instead of paying to store it geologically as a waste (*4*, *5*), considering that such a CO_2 conversion concept offers a promising pathway to recycle carbon within the human socioeconomic system (*6*).

However, the total amount of CO_2 currently converted to chemicals accounts for only about 0.3% of global CO_2 emissions, and more than 90% of it is used for the production of urea (*4*, *7*). Although there have been numerous laboratory approaches for CO_2 conversion developed in recent years, processes capable of using large quantities of CO_2 are still lacking (*4*, *8*). Chemically, conversion of CO_2 requires the introduction of reducing agents to activate the C=O bond in the CO_2 molecule, which leads to the transformation of CO_2 into desired products via the catalyst-assisted rearrangement of chemical bonds in the reducing agent. Therefore, a CO_2 conversion reaction with a reducing agent that is earth abundant and readily available would be of great worth for future technical exploration and development, considering the decarbonization targets of large CO_2 stationary sources worldwide (*9*).

The methane dry reforming (MDR) reaction (Eq. 1), which upgrades CH_4 into syngas, a platform mixture of H_2 and CO that is of great importance to chemical industry, is recently gaining attention (*10*), as it also allows the utilization of CO_2. Methane is a vast but underused resource available in the form of natural gas (hydrate) and shale gas (*3*, *11*), thus offering the MDR reaction a great potential to convert substantial amounts of CO_2 into syngas, which can be transformed into various chemicals or fuels (*12*, *13*). Previous studies on the MDR reaction mostly focused on developing efficient catalysts to facilitate the process chemistry (*14*, *15*), while few of them took into account the source of high-purity CO_2 feedstock required to reform CH_4 in this reaction. Foreseeably, feasible ways for the MDR reaction to be mutually inclusive with CO_2 capture reactions will become the main technical barrier on its way to profitable implementation.

$$CH_4\ (g) + CO_2\ (g) \rightarrow 2CO\ (g) + 2H_2\ (g), \Delta H_{298\ K} = +247.0 kJ\ mol^{-1} \quad (1)$$

As an emerging high-temperature solid-looping CO_2 capture approach, calcium looping (CaL; Eq. 2) (*16*) is attracting interest in designing CO_2-involved chemical processes for energy conversion (*17*, *18*) and storage (*19*, *20*). In the sorption-enhanced catalytic steam reforming of CH_4 (*21*), for example, CaO species is used to shift the CH_4 conversion equilibrium toward higher H_2 production via in situ sorption of CO_2. In these processes, the storage and release of CO_2 can be easily achieved by manipulating its carbonation-decarbonation equilibrium on the CaO-based sorbent. It is acknowledged that the energy penalty to drive highly endothermic reactions, such as $CaCO_3$ calcination and CH_4 dry reforming, is the main challenge faced by current thermochemistry. However, recent advances in solar thermal technology make it a promising alternative to drive the conventional thermochemical processes with concentrated solar heat, which will, in turn, store the solar energy into chemical bonds of the product (*22*, *23*).

$$CaO\ (s) + CO_2\ (g) \leftrightharpoons CaCO_3\ (s), \Delta H_{298\ K} = -178.2 kJ\ mol^{-1} \quad (2)$$

To date, most attention to CCS has been focused on developing separate CO_2 capture (*24*, *25*) or conversion (*26*–*28*) techniques. However, driving forward the CCS strategy requires new concepts for in situ CO_2 utilization by integrating the two technical steps, which has rarely been thought of yet (*29*, *30*). In this study, a novel CaL methane reforming process, which relies on coupling CaL and CH_4 dry reforming via the developed CaO-Ni bifunctional sorbent-catalyst, is put forward to realize the synergetic capture and conversion of CO_2 in one integrated chemical process. Fundamentals of the proposed CaL methane reforming process are studied, CO_2 utilization and CH_4 reforming performance of the process are investigated, and the superiority in reaction kinetics and

[1]School of Engineering, Macquarie University, Sydney, New South Wales 2109, Australia. [2]School of Environmental Science and Engineering, Southern University of Science and Technology, Shenzhen 518055, P. R. China. [3]School of Environment, Tsinghua University, Beijing 100084, P. R. China.
*Corresponding author. Email: sicong.tian@outlook.com

energetics as compared with those of conventional CaL and CH_4 dry reforming processes is demonstrated.

RESULTS

Process description

The most important consideration of the CaL methane reforming process proposed in this study lies in making CO_2 capture and its conversion mutually inclusive in one integrated chemical process. As illustrated in Fig. 1A, the operation of the proposed process relies on the CaO-Ni bifunctional sorbent-catalyst, which is composed of earth-abundant elements. In the CO_2 capture step, CaO in the material separates CO_2 from the gas streams waiting for decarbonization and stores CO_2 in the form of $CaCO_3$. In the CO_2 conversion and CH_4 reforming step, the CO_2 released due to $CaCO_3$ dissociation is used in situ to reform CH_4 on the CaO-Ni interface, producing the syngas with a theoretical H_2-to-CO molar ratio of 1.0. After that, the material returns to the initial state and gets ready for a new CaL CH_4 reforming cycle. One inherent benefit of such a process is that it allows the use of various CO_2-containing gases as a feedstock to reform CH_4, especially the tremendous amount of flue gases with a CO_2 content of no more than 20 volume % that are emitted from coal-fired power plants and large energy-intensive industries. In addition, on account of integrating CO_2 capture with its conversion in one chemical process, the overall energy penalty is expected to be lowered down due to the improved process heat integration and avoidance of CO_2 transportation between its emission source and utilization site.

To better understand the process integration mechanism, we used a sorbent-catalyst composed of only the functional groups, i.e., CaO and metallic Ni (fig. S1A), to drive the proposed process in this study. The metal-support interaction between Ni and CaO in the material was explored by characterizing the chemical state and reducibility of NiO in the freshly calcined sorbent-catalysts (fig. S1B), with different Ca-to-Ni molar ratios as shown in Fig. 2. It was revealed in the x-ray photoelectron spectroscopy (XPS) spectra of Ni $2p_{3/2}$ (Fig. 2A) that the NiO phase exists in two types of chemical states in the material. The XPS peak at ~854 eV is related to the surface NiO that is free from interaction with the CaO support, while the one at a higher binding energy of ~856 eV corresponds to the NiO interacting with CaO. The proportion of the interacted NiO increased from 64.0 to 80.7 atomic % (at %) of the total NiO, with an increasing Ca-to-Ni molar ratio, which was accompanied by a decrease in the proportion of the free NiO. The bimodal H_2-TPR (temperature-programmed reduction) profiles in Fig. 2B indicate the existence of two reducible NiO species in the material, which is in good agreement with the XPS spectra. Reduction of the free NiO species occurred at a lower temperature of ~700 K, and a higher temperature was required to reduce the interacted NiO species. Also, the broader reduction peak of the interacted NiO, as compared to that of the free NiO, indicated that the interaction with the CaO support would lower the reducibility of NiO. Nonetheless, the reduction peaks of NiO supported on CaO occurred at lower temperatures than those on other oxides, including MgO (*31*), Al_2O_3 (*32*), SiO_2 (*33*), and ZnO (*34*), indicative of a stronger reducibility of the sorbent-catalyst prepared in this study than these supported Ni-based catalysts commonly considered for CH_4 reforming. In addition to the metal-support interaction, the textural property of the prepared sorbent-catalysts was also investigated and was identical regardless of the Ca-to-Ni molar ratio in the material (table S1). Taking the freshly reduced CaO/Ni_9 as an example, we can observe that the metallic Ni, which was mostly in a hexagonal shape and with an average crystallite size of 26.7 nm (table S2), was well dispersed in the CaO matrix of the material (Fig. 1, B to D).

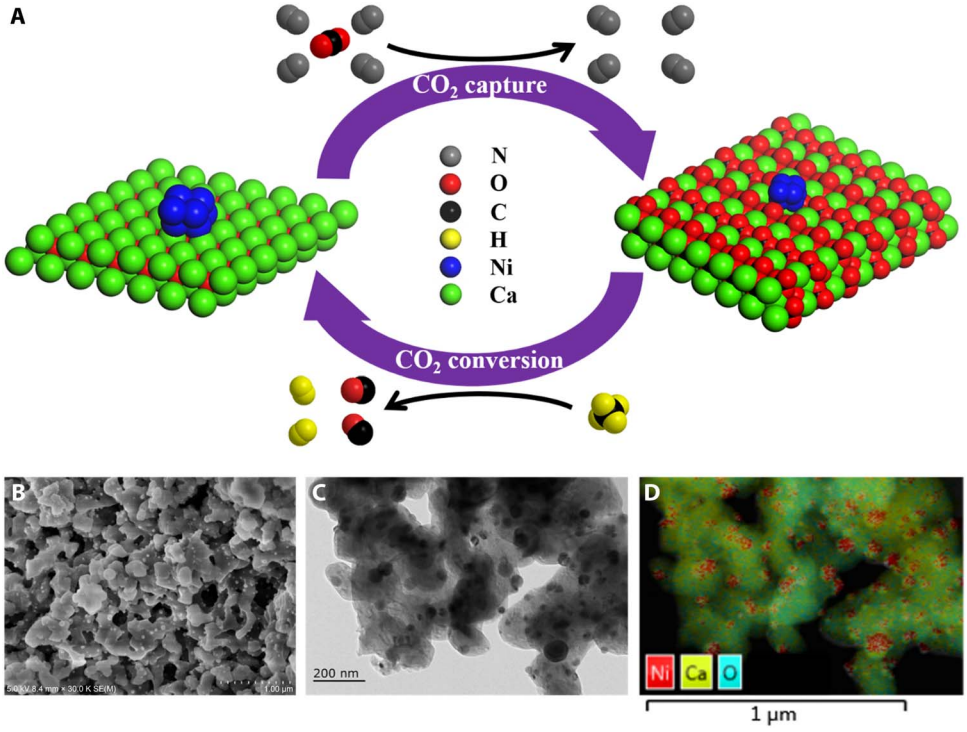

Fig. 1. Illustration of the proposed in situ CO_2 utilization process. (**A**) Process schematic of the catalytic CaL reforming of methane, and the (**B**) micrometer-scale morphology and (**C** and **D**) nanoparticle information of the CaO-Ni bifunctional sorbent-catalyst (freshly reduced CaO/Ni_9) driving the proposed process.

The potential reactions involved in the proposed process were identified through the temperature-programmed surface reactions (TPSRs) on the CaO-Ni interface of the prepared sorbent-catalyst. Figure 3 (A and B) reveals the activation ability of the CaO-Ni interface to CH_4 (reducing agent) and CO_2 (oxidizing agent), respectively. One reaction peak associated with H_2 production was observed at ~900 K in the CH_4-TPSR curve (Fig. 3A), which was indicative of the CH_4 dissociation reaction on the surface of metallic Ni. There were an upward CO_2 capture peak (~940 K) and a downward CO_2 release peak (~1200 K) appearing in the CO_2-TPSR curve (Fig. 3B), corresponding to the CaO carbonation and $CaCO_3$ dissociation reactions, respectively. We can observe that $CaCO_3$ would not begin to dissociate until ~1100 K in an atmosphere containing 20 volume % CO_2; however, the temperature at which $CaCO_3$ dissociation occurred would shift to ~970 K in a N_2 atmosphere (fig. S2). This explained another consideration in designing the proposed process, namely, we attempt to drive $CaCO_3$ dissociation at lower temperatures by exploiting the reaction sensitivity to CO_2 partial pressure in the atmosphere. In addition, the small reaction peak associated with CO production at ~1140 K represented CO_2 oxidation of the metallic Ni (fig. S3), but this reaction appeared to be hard to proceed due to its unfavorable thermodynamics (Fig. 3D).

When CO_2-TPSR was performed on the CaO-Ni interface with deposited carbon after CH_4-TPSR (Fig. 3C), the reaction curve derived was significantly different from that in Fig. 3B. After the CaO carbonation reaction in region 1, consumption of CO_2 in the atmosphere went on all through region 2, unlike the situation in Fig. 3B, where the CO_2 consumption reaction ceased gradually. This indicated the occurrence of the reverse Boudouard reaction between CO_2 in the atmosphere and the deposited carbon on the CaO-Ni interface, considering the observation that the CO intensity kept increasing in this region. As the temperature increased, the TPSR curve exhibited an overlap between the upward CO_2 consumption and the downward CO_2 release peaks in

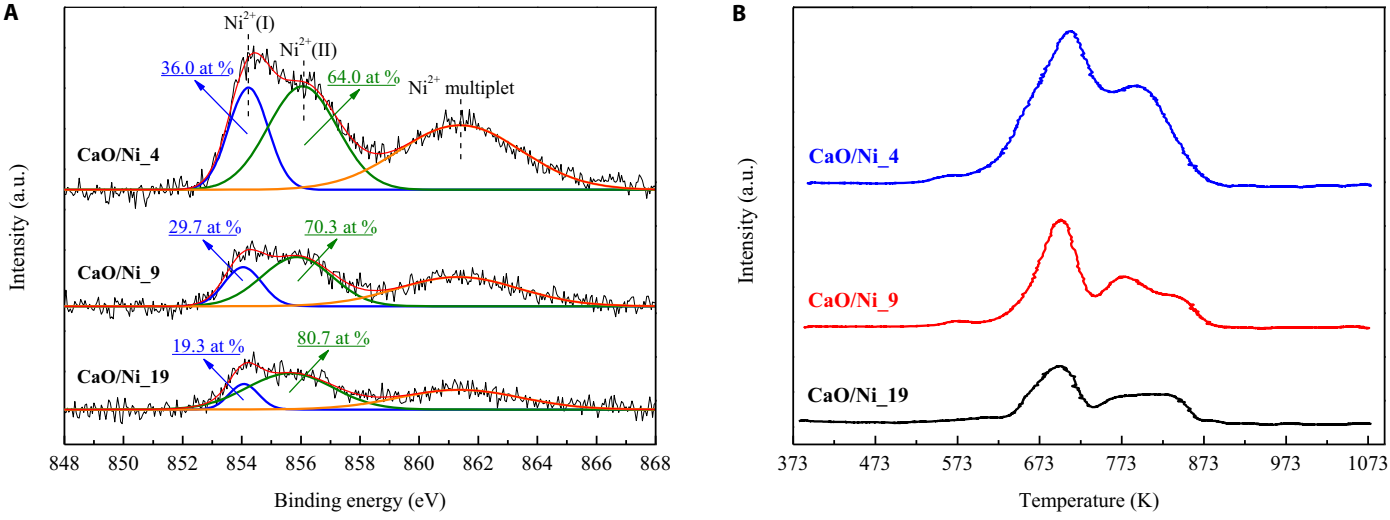

Fig. 2. Metal-support interaction in the material. (**A**) XPS spectra corresponding to Ni $2p_{3/2}$ and (**B**) H_2-TPR profiles of the prepared CaO-Ni bifunctional sorbent-catalysts. a.u., arbitrary units.

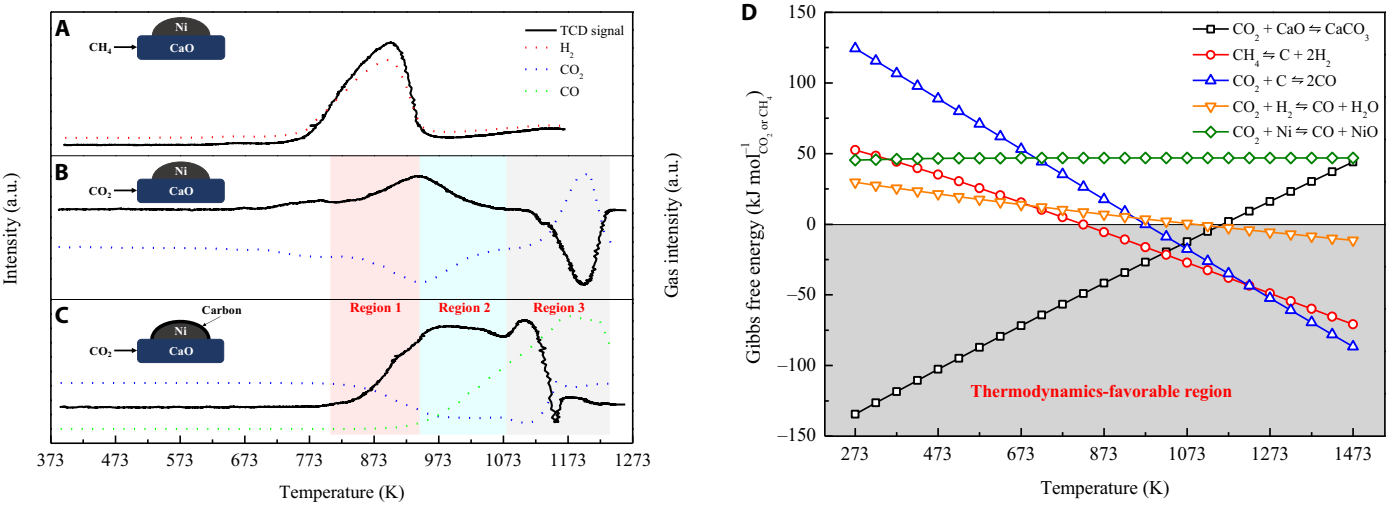

Fig. 3. Reaction identification on the CaO-Ni interface. (**A** to **C**) Temperature-programmed reactions on the surface of freshly reduced CaO/Ni_9 to identify the coupling reactions involved in the CaL methane reforming process. (**D**) Gibbs free energy of related reactions as a function of temperature.

region 3, where the CO_2 peak in Fig. 3B was fully replaced by the CO peak in Fig. 3C. This suggested a good integration of the $CaCO_3$ dissociation and reverse Boudouard reactions, resulting in the reduction of the CO_2 released from $CaCO_3$ into CO on the CaO-Ni interface. It was, furthermore, revealed that the reverse Boudouard reaction between the CO_2 released due to $CaCO_3$ dissociation and the deposited carbon formed due to CH_4 dissociation contributes the most to CO_2 conversion among all the CO_2 reduction reactions occurring in the CaL methane reforming process proposed. This conclusion can also be drawn from the reaction thermodynamics point of view. As shown in Fig. 3D, the Gibbs free energy of the reverse Boudouard reaction is much lower than those of other CO_2 reduction reactions in the temperature region investigated, indicative of an easier occurrence of such a reaction. In addition, it was observed that the temperature at which H_2 was generated in Fig. 3A was appreciably lower than that of CO in Fig. 3C, indicating that the CaO-Ni interface in the material is better able to activate CH_4 than CO_2. This is likely because the CH_4 dissociation reaction is less endothermic than the reverse Boudouard reaction (fig. S4).

Performance of CO_2 utilization and CH_4 reforming

An experimental demonstration of the proposed CaL methane reforming process is shown in Fig. 4. Using the sorbent-catalyst CaO/Ni_9, the syngas yield could reach a maximum of 10.4 mmol $g_{sorb.-cat.}^{-1}$ at cycle 2 and exhibited a marginal decrease with the cycle number (Fig. 4A). This is attributed to the decrease in the cyclic CO_2 capture capacity of the material in the CO_2 capture step (fig. S5A), which would result in less CO_2 being available for CO production in the following CO_2 conversion step. Alternatively, strengthening the metal-support interaction (*35*) and/or the confinement effect of support (*36*) in the material matrix could be considered to improve the sintering resistance of the material in the process. Nonetheless, the experimentally determined H_2-to-CO molar ratio of the syngas produced through the proposed process stabilized at about 1.1 for most cycles and was a bit higher than the theoretical ratio of 1.0 through conventional MDR. As discussed above, this is probably because the CaO-Ni interface in the material is more in favor of the CH_4 dissociation reaction to yield H_2 than the CO_2 reduction reactions to yield CO. It was shown in Fig. 4B that CH_4 conversion of the proposed process exceeded 80% over the cycles investigated and was higher than that of conventional MDR (*37*, *38*) and comparable with those of other novel CH_4 reforming processes (*17*, *18*, *39*, *40*). However, CO_2 conversion was notably lower than CH_4 conversion in the process. This is reasonable because the CO_2 conversion reported here represents the proportion of CO_2 that is stored in the capture step and then reduced in the conversion step; therefore, the incomplete capture of CO_2 in the

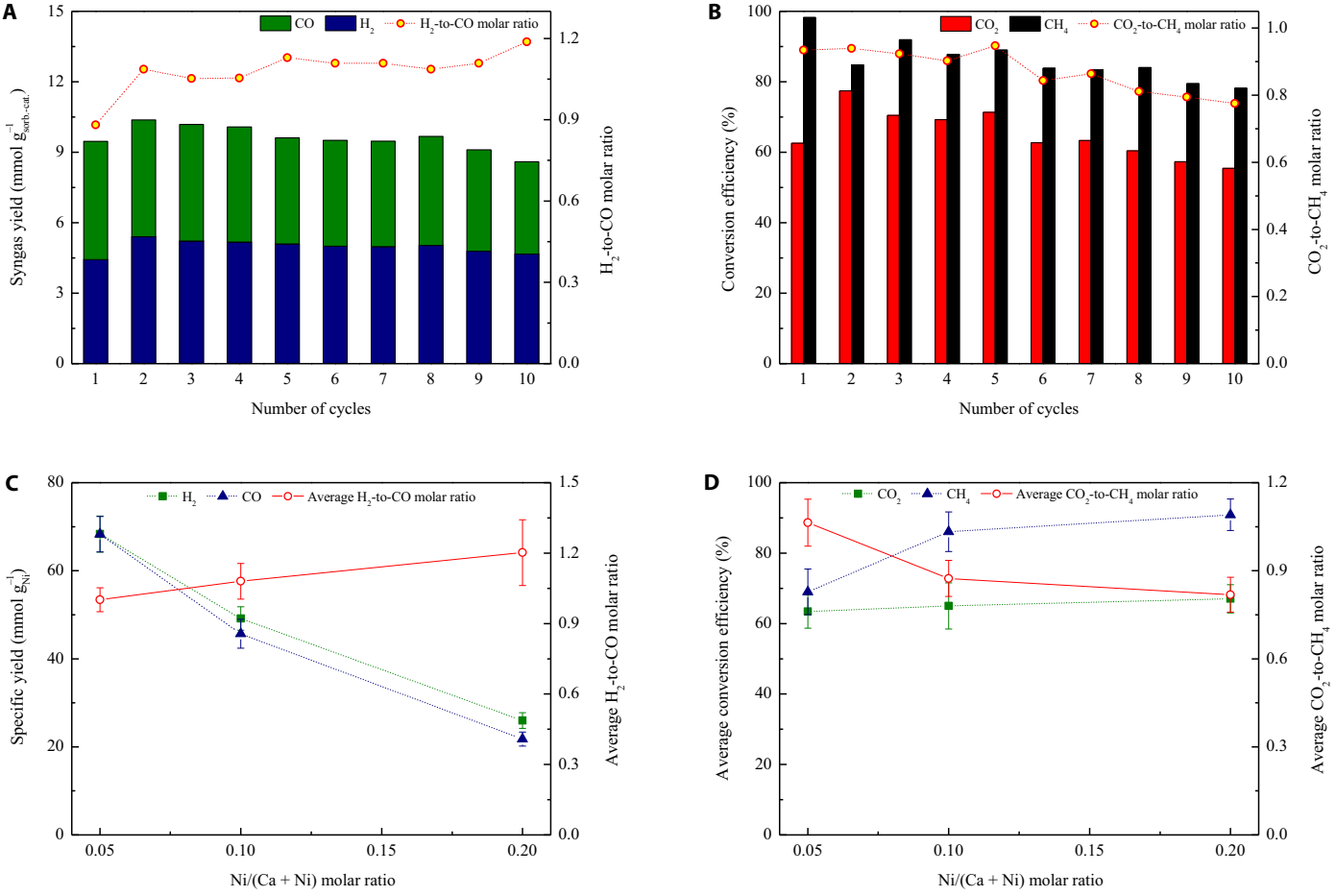

Fig. 4. Reaction studies of the CaL methane reforming process. (**A**) Syngas yield and H_2-to-CO molar ratio and (**B**) conversion efficiency of CO_2 and CH_4 along with their consumption molar ratio as a function of the cycle number using CaO/Ni_9. (**C**) Specific yield of H_2 and CO (average yield per gram of the loaded Ni) along with their molar ratio and (**D**) average conversion efficiency of CO_2 and CH_4 along with their average consumption molar ratio during the 10 cycles as a function of the Ni/(Ca + Ni) molar ratio in the sorbent-catalyst.

atmosphere results in the gap between the conversions of CO_2 and CH_4 (fig. S5B). Actually, the consumptions of CO_2 and CH_4 were very close in the proposed process, allowing the CO_2-to-CH_4 molar ratio to approach 1.0 at the beginning cycles. In addition to the enhancement in sintering resistance of the material, improved CH_4 and CO_2 conversions can be achieved by changing the reactor configuration from the packed-bed to fluidized-bed operation (*16*, *41*, *42*).

The elemental availability of the CaO-Ni bifunctional sorbent-catalyst used for the proposed process was studied by varying the Ni/(Ca + Ni) molar ratio in the material (Fig. 4, C and D). The average H_2 and CO yields of the material increased from 3.5 to 5.1 mmol $g_{sorb.-cat.}^{-1}$ for H_2 and from 3.5 to 4.6 mmol $g_{sorb.-cat.}^{-1}$ for CO with an increasing Ni/(Ca + Ni) molar ratio (fig. S6A). However, the situation was contrary when the average H_2 and CO yields were considered on the basis of per gram of the loaded Ni in the material (Fig. 4C), namely, the specific yield of both H_2 and CO as derived would decrease with the increase of the Ni/(Ca + Ni) molar ratio. Such a contrary situation was also observed when comparing the change in average CO_2 and CH_4 consumptions (fig. S6B) with that in their specific consumptions (fig. S7). These observations can be explained by the Ni availability in the material, where the surface area of metallic Ni per gram of the material increased with the Ni/(Ca + Ni) molar ratio but would decrease once calculated as the area per gram of the loaded Ni in the material (table S3). As shown in Fig. 4D, the conversions of CO_2 and CH_4 could be increased to 67 and 91%, respectively, but this would come at the cost of the catalytic efficiency of metallic Ni in the material. In addition, an increase in the H_2-to-CO molar ratio of the syngas produced (Fig. 4C) and a decrease in the CO_2-to-CH_4 consumption molar ratio (Fig. 4D) were observed as the Ni/(Ca + Ni) molar ratio increased. This is conceivable on the basis of the above discussions, because a higher content of Ni in the material will lead to more consumption of CH_4 for H_2 production, while a lower content of CaO in the material will result in less consumption of CO_2 for CO production. As with other CH_4 reforming processes (*43*–*45*), the CaL methane reforming process proposed is faced with the issue of carbon deposition, which is revealed to be a result of the thermodynamic and kinetic differences between the reverse Boudouard and CH_4 dissociation reactions in this study. There was more carbon deposited in the material with a higher Ni/(Ca + Ni) molar ratio (fig. S8). However, the type of the deposited carbon remained unchanged. The formation of filamentous carbon around Ni nanoparticles was observed in the transmission electron microscopy (TEM) images of spent sorbent-catalysts (fig. S9, A and B), and the presence of two carbon species was confirmed in the Raman spectra of spent sorbent-catalysts (fig. S9C). They were the species at G band (~1580 cm^{-1}) and D band (~1330 cm^{-1}), which are related to the graphitic carbon and its defective structures, respectively (*46*). Therefore, from the perspective of material design, the CaO-Ni bifunctional sorbent-catalyst developed in this study has room to be improved in terms of the carbon-resistant ability, which could be achieved by manipulating the particle size of metallic Ni (*47*) and/or using the bimetallic Ni-based catalysts (*48*).

Superiority in process kinetics and energetics

A selected region (2θ, 28° to 34°) of the time-resolved in situ x-ray diffraction (XRD) patterns, indicating the change in diffraction intensity of the $CaCO_3$ (104) surface (2θ = 29.400°) and the CaO (111) surface (2θ = 32.228°) during material decarbonation, is shown in contour plots in Fig. 5 (A to C). As can be seen, the diffraction intensity of the $CaCO_3$ (104) surface did not exhibit a notable decrease with time in either a N_2 (Fig. 5A) or a CH_4 (Fig. 5B) atmosphere, revealing that the $CaCO_3$ dissociation reaction for CO_2 release occurred slowly. Therefore, to achieve favorable decarbonation kinetics in the atmosphere with high CO_2 partial pressures, conventional CaL has to be operated at elevated temperatures above 1173 K. However, this comes at the cost of a decay in the CO_2 capture capacity of all CaO-based sorbents due to high-temperature sintering, which is the most serious problem restricting the development of such a process for CO_2 capture (*49*). When metallic Ni appeared in the $CaCO_3$ matrix (Fig. 5C), the $CaCO_3$ dissociation reaction was significantly accelerated when compared to the case of separate $CaCO_3$ in Fig. 5B, because the $CaCO_3$ (104) surface disappeared rapidly, accompanied

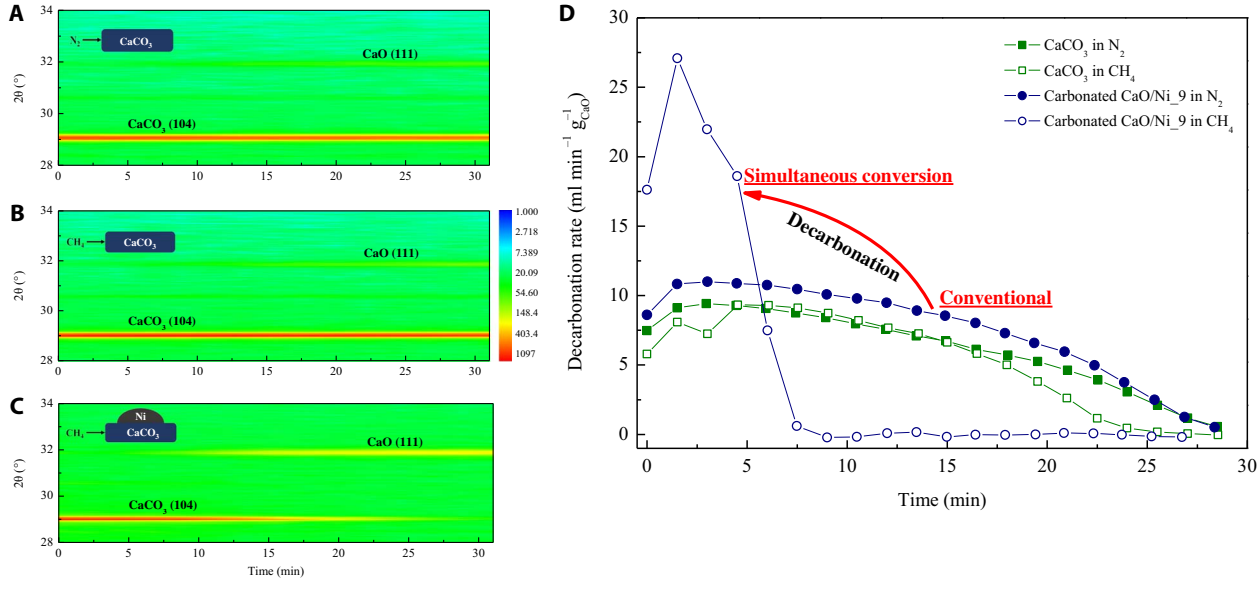

Fig. 5. Comparison of decarbonation kinetics between the CaL methane reforming and separate CaL processes. In situ XRD characterization for isothermal decarbonation of (**A**) $CaCO_3$ in a N_2 atmosphere, (**B**) $CaCO_3$ in a CH_4 atmosphere, and (**C**) carbonated CaO/Ni_9 in a CH_4 atmosphere at 1073 K. (**D**) Decarbonation rate as a function of time at 1073 K.

by the appearance of the CaO (111) surface. This phenomenon is attributed to the effect of Le Chatelier's principle. Namely, the continuous consumption of the CO_2 released from $CaCO_3$ to reform CH_4 on the adjacent metallic Ni will shift the thermodynamic equilibrium of the $CaCO_3$ dissociation reaction, providing an additional driving force for material decarbonation. As depicted in Fig. 5D, when Ni-catalyzed CH_4 reforming was not involved, decarbonation of the $CaCO_3$ reference and the carbonated CaO/Ni_9 proceeded at close but slow reaction rates. However, when Ni-catalyzed CH_4 reforming was integrated with $CaCO_3$ calcination, the decarbonation rate of the material was sharply increased, shortening the time required to accomplish the $CaCO_3$ dissociation reaction to almost a quarter of that required for separate $CaCO_3$ calcination. This is encouraging, because we have a chance to operate the energy-intensive $CaCO_3$ calcination at lower temperatures but with superior reaction kinetics, thus mitigating the issue of material deactivation caused by high-temperature sintering.

The energetics of the proposed CaL methane reforming process was estimated in terms of energy efficiency and fuel economy, as shown in Fig. 6. The energy consumption for CO_2 utilization (Fig. 6A), indicative of the process energy efficiency, reduces with the decrease of the carbonation temperature and increase of the calcination temperature up to 1173 K. This is determined by thermodynamics of the coupling reactions in the proposed process, where equilibrium conversion of the exothermic CaO carbonation reaction for CO_2 capture decreases with the increase of temperature, while the endothermic CO_2 reduction reactions are facilitated at higher temperatures (fig. S10). The region on the left of the black curve in Fig. 6A represents the conditions under which the utilization of CO_2 through the proposed process is more energy efficient than that through conventional MDR with the CO_2 supplied by conventional CaL. Especially when the carbonation temperature is below 900 K, the proposed process is energy efficient regardless of the change in calcination temperature. It is important that the lowest energy consumptions for CO_2 utilization of the proposed CaL methane reforming process are achieved at carbonation temperatures of ~873 K and calcination temperatures of ~1173 K, which are within the range of operating temperatures of conventional MDR and CaL.

When we turn to the fuel economy, the fuel requirement for syngas production (Fig. 6B) considered here includes the amount of CH_4 consumed for both chemical synthesis and process heat. As can be seen, the fuel requirement for syngas production increases with the carbonation temperature but decreases with the calcination temperature. The region above the black curve in Fig. 6B represents the conditions under which less fuel (CH_4) is required in the proposed process than in conventional MDR with the CO_2 supplied by conventional CaL. When the calcination temperature is above 1023 K, the proposed process begins to be superior to the combination of conventional MDR and CaL processes in terms of the total CH_4 consumed per mole of syngas produced. In addition, it is revealed in Fig. 6 that the energy consumption for CO_2 utilization is mainly influenced by the carbonation temperature, while the fuel requirement for syngas production is mainly influenced by the calcination temperature. This is not surprising when we realize that the CO_2 converted in the proposed process comes from that captured during the carbonation stage, and syngas production depends highly on the CH_4 reforming efficiency during the calcination stage. Under the conditions investigated in this study, the energy consumption for CO_2 utilization (534.8 kJ $mol_{CO_2}^{-1}$) and the fuel requirement for syngas production (0.521 mol_{CH_4} mol_{syn}^{-1}) are 22 and 9% lower, respectively, than those of conventional processes. Therefore, it is clear that, in addition to the superiority in process kinetics, the thermodynamic cooperativity of the coupling reactions involved in the proposed process results in an appreciably improved energy efficiency compared to the combination of conventional MDR and CaL processes.

DISCUSSION

A novel thermochemical process for in situ CO_2 utilization, i.e., CaL reforming of methane, is put forward and experimentally demonstrated in this study to effectively combine CO_2 capture with its conversion. On account of integrating CaL CO_2 capture into MDR via the CaO-Ni bifunctional sorbent-catalyst developed, the proposed process is capable of using various CO_2-containing gases as a feedstock to reform CH_4, offering a chance to directly utilize the CO_2 emitted in enormous quantities from its large stationary sources. Using the sorbent-catalyst

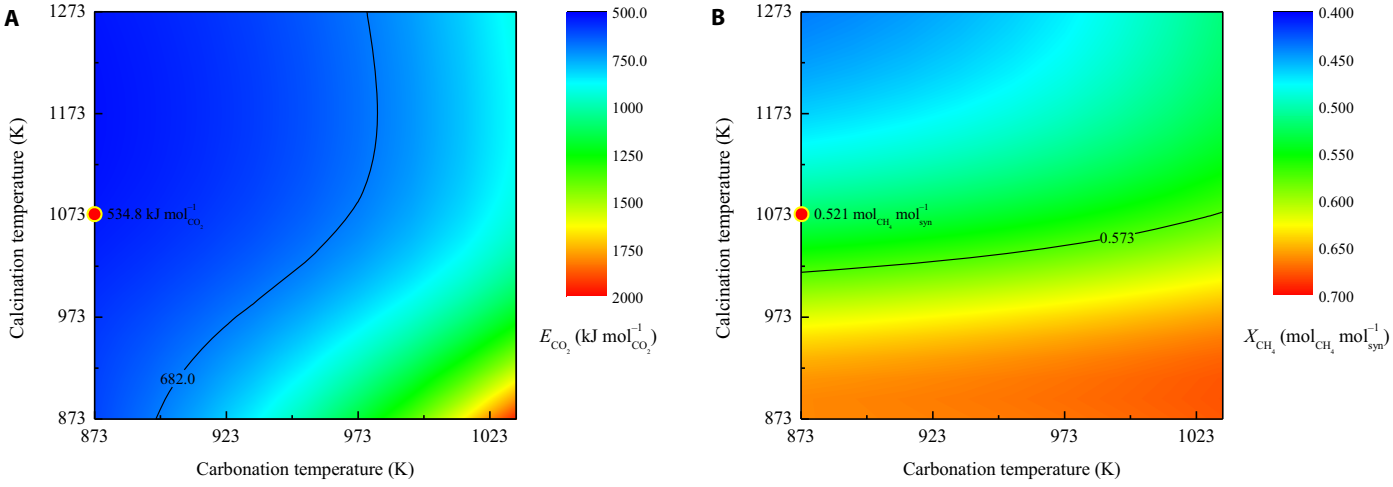

Fig. 6. Energetics of the CaL methane reforming process. (**A**) Energy consumption for CO_2 utilization (E_{CO_2}, kilojoules per mole of CO_2 converted) and (**B**) fuel requirement for syngas production (X_{CH_4}, moles of CH_4 consumed per mole of syngas produced) as a function of carbonation and calcination temperatures. The black curve indicates the value corresponding to the application of conventional MDR using the CO_2 supplied by conventional CaL. The solid red circle indicates the value corresponding to the operating temperatures of the CaL methane reforming process investigated in this study.

CaO/Ni_9, the proposed process could result in an average cyclic CO_2 utilization efficiency of 65% under the investigated conditions; meanwhile, the average cyclic CH_4 conversion (86%) is competitive against those of conventional MDR and other novel CH_4 reforming processes. In addition, the proposed process integration concept provides mutual benefits between the CaL CO_2 capture and the MDR reactions. On the one hand, the in situ consumption of CO_2 through the MDR reaction drives the $CaCO_3$ dissociation reaction according to Le Chatelier's principle, allowing such an energy-intensive reaction to be operated with superior reaction kinetics at lower temperatures as compared to those of conventional CaL and thus mitigating the sintering-caused material deactivation that is a common issue restricting the development of the CaL-based CO_2 capture technology. On the other hand, due to the introduction of the CaO-based CO_2-carrying cycle, the energy consumption for CO_2 utilization and the fuel requirement for syngas production of the proposed process are 22 and 9% lower, respectively, than those of conventional MDR. The CaL methane reforming process proposed in this study uses a reductant (CH_4) and a material (CaO-Ni bifunctional sorbent-catalyst), which are earth abundant to achieve in situ CO_2 conversion, offering a promising option to close the anthropogenic carbon cycle directly at large CO_2 stationary sources.

MATERIALS AND METHODS

Sorbent-catalyst preparation

The CaO-Ni bifunctional sorbent-catalyst was prepared via the well-known Pechini sol-gel method (*50*, *51*) using metal nitrates, citric acid (CA), and ethylene glycol (EG) at a molar ratio of 1:2:2. In a typical synthesis, calculated amounts of $Ca(NO_3)_2{\cdot}4H_2O$, $Ni(NO_3)_2{\cdot}6H_2O$, and anhydrous CA were dissolved in deionized water, and the as-prepared solution was magnetically stirred at 348 K in an oil bath for 1 hour to form the metal-CA chelates. Then, EG was added to the solution, with the temperature of the resulting solution increased to 363 K. Gelation of the solution occurred through the poly-esterification reaction between EG and metal-CA chelates at 363 K with continuous stirring until the removal of excess solvent. The obtained gel was dried overnight at 373 K in an oven and then calcined at 1073 K for 2 hours. The as-synthesized sorbent-catalysts were labeled as CaO/Ni_*x*, where *x* denotes the molar ratio of Ca to Ni in the material. In some cases, the material was fully reduced by H_2 at 1073 K for 3 hours before use (table S2). In addition to the CaO-Ni bifunctional sorbent-catalysts, pure CaO without the loading of Ni was prepared, according to the abovementioned procedures, for comparison.

Sorbent-catalyst characterization

Nitrogen physisorption was performed to determine the Brunauer-Emmett-Teller surface area, Barrett-Joyner-Halenda pore volume, and the pore and particle sizes of the prepared sorbent-catalysts in an automated surface area and porosity analyzer (TriStar II 3020, Micromeritics) at 77 K. Before the experiment, each sample was degassed at 573 K for 4.5 hours. CO pulse chemisorption was performed to determine the surface area and dispersion of metallic Ni in the freshly reduced sorbent-catalysts in an automated chemisorption analyzer (AutoChem II 2920, Micromeritics) at 323 K. During the experiment, CO pulses (10 volume % CO in He) were introduced until the adsorption was complete and the total amount of CO consumed was recorded. On the basis of this, the surface area and dispersion were calculated assuming that the Ni:CO stoichiometry factor was 1.0 and the atomic cross-sectional area was 0.0649 nm^2.

Powder XRD was performed in the 2θ range of 10° to 80° (step size: 0.02° and time per step: 0.33 s) to identify the crystalline phases in the sorbent-catalysts using an x-ray diffractometer (D8 Advance, Bruker AXS) with Cu Kα radiation. The content and crystallite size of metallic Ni in the materials were determined on the basis of Rietveld refinement of the as-acquired XRD patterns using the TOPAS software (version 4.2, Bruker AXS) (*52*). XPS was performed to obtain chemical information on the surface of the sorbent-catalysts in an x-ray photoelectron spectrometer (ESCALAB 250Xi, Thermo Fisher Scientific) equipped with a monochromatized Al Kα source. The XPS spectrum corresponding to Ni $2p_{3/2}$ was measured within a binding energy range of 848 to 868 eV. The multiple spectral peaks in the as-acquired spectrum were fitted on the basis of a Gaussian function and then identified according to the National Institute of Standards and Technology (NIST) database (*53*). The morphology and nanoparticle information of the freshly reduced sorbent-catalyst were observed using a scanning electron microscope (S-4800, Hitachi) and a field-emission transmission electron microscope (JEM-2100F, JEOL) equipped with a JED-2300 Silicon Drift Detector energy-dispersive x-ray spectrometer, respectively.

TPSRs were performed in an automated chemisorption flow analyzer (ChemBET PULSAR TPR/TPD, Quantachrome Instruments), and two separate programs were executed to characterize the prepared sorbent-catalyst. For program I, a small amount of the freshly calcined sorbent-catalyst (~50 mg) was placed in a quartz U-tube and heated to 1073 K at a rate of 10 K min^{-1} under a gas flow of 50 ml min^{-1} containing 5 volume % H_2 (balance in N_2). Upon cooling to 373 K under a N_2 flow, the sample was heated to 1173 K at a rate of 10 K min^{-1} under a gas flow of 50 ml min^{-1} containing 5 volume % CH_4 (balance in N_2). After that, the sample was cooled to 373 K under a N_2 flow and then heated to 1273 K at a rate of 10 K min^{-1} under a gas flow of 50 ml min^{-1} containing 20 volume % CO_2 (balance in N_2). For program II, another ~50 mg of the freshly calcined sorbent-catalyst was placed in a quartz U-tube. After H_2-TPR, as described in the first heating procedure of program I, the sample was cooled to 373 K under a N_2 flow and then directly heated to 1273 K at a rate of 10 K min^{-1} under a gas flow of 50 ml min^{-1} containing 20 volume % CO_2 (balance in N_2). During each heating period, the change in the thermal conductivity of the gas flow passing through the sample was continuously recorded using a chemisorption analyzer.

Carbon deposition on spent sorbent-catalysts was characterized using a Raman microscope (LabRAM HR Evolution, Horiba Scientific). The Raman spectra were acquired in the band range of 500 to 3500 cm^{-1} using a laser with a wavelength of 633 nm. Thermogravimetric analysis (TGA) was further performed to quantify the deposited carbon by calculating the difference in weight range between the freshly reduced and spent sorbent-catalysts during oxidation in an air atmosphere at 1073 K for 45 min in a thermogravimetric analyzer (TGA/DSC 2, Mettler Toledo).

Process tests

The proposed CaL methane reforming process was tested using the prepared CaO-Ni bifunctional sorbent-catalysts in a ChemBET PULSAR TPR/TPD chemisorption analyzer. Approximately 0.1 g of the sorbent-catalyst was placed in a quartz U-tube and heated to 1073 K at a rate of 25 K min^{-1} under a N_2 flow of 8 ml min^{-1}. Then, the temperature was held for 60 min with the introduction of H_2 (2 ml min^{-1}) to reduce the sample. After that, the temperature was decreased to 873 K, followed by the introduction of a CO_2 flow of 2 ml min^{-1} instead of the H_2 flow to carbonate the sample for 6 min (the CO_2 capture step). Then, the temperature was increased to 1073 K at a rate of 40 K min^{-1}, followed by the

introduction of a CH_4 flow of 2 ml min^{-1} instead of the CO_2 flow to calcine the sample for 6 min (the CO_2 conversion and CH_4 reforming step). Subsequently, the temperature was decreased to 873 K, and then a new CaL CH_4 reforming cycle was started by the introduction of a CO_2 flow. Ten CaL CH_4 reforming cycles were investigated in this study, and a blank run was performed to correct for the effects of temperature and gas flow switches. During the whole experiment, concentrations of CO_2, CH_4, and H_2 in the outlet gas from the reaction tube were monitored every 1.2 min using a micro-gas chromatograph (GC; 490-GC, Varian), while the concentration of CO in the outlet gas was monitored every 1.2 min using another GC (7890B, Agilent). Both the Varian micro-GC and the Agilent GC were equipped with a molecular sieve 5A column and a thermal conductivity detector (TCD).

In situ XRD experiments were performed in a Bruker D8 Advance x-ray diffractometer to compare the process decarbonation kinetics of CaL reforming of methane and separate CaL. The diffractometer was equipped with an Anton Paar XRK 900 reactor chamber, which enables the XRD investigation of solid-state or solid-gas reactions under controlled temperatures and atmospheres. During the experiment, an appropriate amount of the powder sample, resting on a ceramic-sieve holder, was placed in the reactor chamber and heated to 873 K at a rate of 10 K min^{-1} in a N_2 atmosphere. Once the reaction temperature was reached, a gas flow containing 20 volume % CO_2 (balance in N_2) was introduced into the reactor chamber to carbonate the sample for 30 min. After that, the temperature was increased to 1073 K, and then the atmosphere was switched to a N_2 flow or a gas flow containing 20 volume % CH_4 (balance in N_2), with the sample held at this temperature for another 30 min, during which the time-resolved XRD data of the sample were acquired in the 2θ range of 27° to 47° at a scanning rate of 10° min^{-1}. In addition, the decarbonation rate of the materials during both processes was determined by carrying out the in situ XRD experimental procedures mentioned above in the chemisorption analyzer, and concentrations of CO_2 and CO in the outlet gas during isothermal decarbonation were monitored using the Varian 490 micro-GC and the Agilent 7890B GC, respectively.

Thermodynamic calculations

The HSC Chemistry software (version 6.0, Outotec Technologies) was used in this study to calculate the Gibbs free energy, enthalpy, and thermodynamic equilibrium of related reactions according to the criterion of Gibbs free energy minimization. On the basis of these thermodynamic calculations, the energy consumption for CO_2 utilization (E_{CO_2}, kJ $mol^{-1}_{CO_2}$) and fuel requirement for syngas production (X_{CH_4}, mol_{CH_4} mol^{-1}_{syn}) of the proposed CaL methane reforming process can be determined via Eqs. 3 and 4, respectively, once an initial amount of reactants and the corresponding carbonation and calcination temperatures are specified.

$$E_{CO_2}(T_1, T_2) = \frac{\sum E_{\text{Reaction i}} + \sum E_{\text{Reactant k}}}{n^1_{CO_2} - [n]^1_{CO_2} - [n]^2_{CO_2} - [n]^2_{CaCO_3}} \quad (3)$$

$$X_{CH_4}(T_1, T_2) = \frac{\left(\sum E_{\text{Reaction i}} + \sum E_{\text{Reactant k}}\right)/HHV_{CH_4} + n^2_{CH_4} - [n]^2_{CH_4}}{[n]^2_{H_2} + [n]^2_{CO}} \quad (4)$$

where $E_{\text{Reaction i}}$ (kJ) and $E_{\text{Reactant k}}$ (kJ) represent the energy required to drive the chemical reaction i and heat the related reactant k to the carbonation temperature (T_1, K) or calcination temperature (T_2, K), respectively. n^1_k (mol) and $[n]^1_k$ (mol) represent the initial and equilibrium amounts of the reaction species k, respectively, at the carbonation step, while n^2_k (mol) and $[n]^2_k$ (mol) represent those at the calcination step. HHV_{CH_4} represents the high heat value of methane (kJ mol^{-1}).

The terms $E_{\text{Reaction i}}$ and $E_{\text{Reactant k}}$ in the above equations can be determined via Eqs. 5 and 6, respectively.

$$E_{\text{Reaction i}} = (n_k - [n]_k) \cdot \Delta H_i \quad (5)$$

$$E_{\text{Reactant k}} = n_k \cdot \int CP_k(T) \cdot dT \quad (6)$$

where ΔH_i (kJ mol^{-1}) and CP_k (kJ mol^{-1} K^{-1}) represent the enthalpy of reaction i and the heat capacity of reactant k, respectively.

SUPPLEMENTARY MATERIALS

Supplementary material for this article is available at http://advances.sciencemag.org/cgi/content/full/5/4/eaav5077/DC1

Fig. S1. X-ray diffraction characterization of the prepared sorbent-catalysts.
Fig. S2. Temperature-programmed carbonation-decarbonation profile of CaO.
Fig. S3. Intensity of TCD signal and CO as a function of temperature during CO_2-TPSR on the surface of freshly reduced CaO/Ni_9.
Fig. S4. Enthalpy of main reactions involved in the proposed CaL methane reforming process.
Fig. S5. CO_2 capture performance of the prepared sorbent-catalysts in the CaL methane reforming process.
Fig. S6. Influence of the Ni/(Ca + Ni) molar ratio on the performance of the CaL methane reforming process.
Fig. S7. Specific CO_2 and CH_4 consumption as a function of the Ni/(Ca + Ni) molar ratio in the sorbent-catalyst.
Fig. S8. Thermogravimetric quantification of the deposited carbon in the spent sorbent-catalysts.
Fig. S9. Carbon deposition characteristics of the prepared CaO-Ni bifunctional sorbent-catalysts.
Fig. S10. Thermodynamic equilibrium of related reactions involved in the CaL methane reforming process.
Table S1. Nitrogen physisorption results of the freshly calcined sorbent-catalysts.
Table S2. The content and crystallite size of metallic Ni in the freshly reduced sorbent-catalysts.
Table S3. CO pulse chemisorption results of the freshly reduced sorbent-catalysts.

REFERENCES AND NOTES

1. J. Rogelj, M. den Elzen, N. Höhne, T. Fransen, H. Fekete, H. Winkler, R. Schaeffer, F. Sha, K. Riahi, M. Meinshausen, Paris agreement climate proposals need a boost to keep warming well below 2°C. *Nature* **534**, 631–639 (2016).
2. International Energy Agency, *Energy Technology Perspectives 2016: Towards Sustainable Urban Energy Systems* (International Energy Agency, 2016).
3. International Energy Agency, *Energy Technology Perspectives 2012: Pathways to a Clean Energy System* (International Energy Agency, 2012); www.iea.org/publications/freepublications/publication/ETP2012_free.pdf.
4. A. Otto, T. Grube, S. Schiebahn, D. Stolten, Closing the loop: Captured CO_2 as a feedstock in the chemical industry. *Energy Environ. Sci.* **8**, 3283–3297 (2015).
5. J. C. Abanades, E. S. Rubin, M. Mazzotti, H. J. Herzog, On the climate change mitigation potential of CO_2 conversion to fuels. *Energy Environ. Sci.* **10**, 2491–2499 (2017).
6. M. He, Y. Sun, B. Han, Green carbon science: Scientific basis for integrating carbon resource processing, utilization, and recycling. *Angew. Chem. Int. Ed.* **52**, 9620–9633 (2013).
7. The World Bank (2018); https://data.worldbank.org/indicator/EN.ATM.CO2E.KT.
8. M. Aresta, A. Dibenedetto, A. Angelini, Catalysis for the valorization of exhaust carbon: From CO_2 to chemicals, materials, and fuels. Technological use of CO_2. *Chem. Rev.* **114**, 1709–1742 (2014).
9. International Energy Agency, *20 Years of Carbon Capture and Storage—Accelerating Future Deployment* (International Energy Agency, 2016); www.iea.org/publications/freepublications/publication/20YearsofCarbonCaptureandStorage_WEB.pdf.
10. S. M. Kim, P. M. Abdala, T. Margossian, D. Hosseini, L. Foppa, A. Armutlulu, W. van Beek, A. Comas-Vives, C. Copéret, C. Müller, Cooperativity and dynamics increase the performance of NiFe dry reforming catalysts. *J. Am. Chem. Soc.* **139**, 1937–1949 (2017).

11. U.S. Energy Information Administration, *Annual Energy Outlook 2014 with Projections to 2040* (U.S. Energy Information Administration, 2014); www.eia.gov/outlooks/aeo/pdf/0383(2014).pdf.
12. H. Xiong, L. L. Jewell, N. J. Coville, Shaped carbons as supports for the catalytic conversion of syngas to clean fuels. *ACS Catal.* **5**, 2640–2658 (2015).
13. H. T. Luk, C. Mondelli, D. C. Ferré, J. A. Stewart, J. Pérez-Ramírez, Status and prospects in higher alcohols synthesis from syngas. *Chem. Soc. Rev.* **46**, 1358–1426 (2017).
14. D. Pakhare, J. Spivey, A review of dry (CO_2) reforming of methane over noble metal catalysts. *Chem. Soc. Rev.* **43**, 7813–7837 (2014).
15. S. Kawi, Y. Kathiraser, J. Ni, U. Oemar, Z. Li, E. T. Saw, Progress in synthesis of highly active and stable nickel-based catalysts for carbon dioxide reforming of methane. *ChemSusChem* **8**, 3556–3575 (2015).
16. D. P. Hanak, E. J. Anthony, V. Manovic, A review of developments in pilot-plant testing and modelling of calcium looping process for CO_2 capture from power generation systems. *Energy Environ. Sci.* **8**, 2199–2249 (2015).
17. L. C. Buelens, V. V. Galvita, H. Poelman, C. Detavernier, G. B. Marin, Super-dry reforming of methane intensifies CO_2 utilization via Le Chatelier's principle. *Science* **354**, 449–452 (2016).
18. M. Kathe, A. Empfield, P. Sandvik, C. Fryer, Y. Zhang, E. Blair, L.-S. Fan, Utilization of CO_2 as a partial substitute for methane feedstock in chemical looping methane–steam redox processes for syngas production. *Energy Environ. Sci.* **10**, 1345–1349 (2017).
19. D. P. Hanak, C. Biliyok, V. Manovic, Calcium looping with inherent energy storage for decarbonisation of coal-fired power plant. *Energy Environ. Sci.* **9**, 971–983 (2016).
20. V. V. Galvita, H. Poelman, G. B. Marin, Combined chemical looping for energy storage and conversion. *J. Power Sources* **286**, 362–370 (2015).
21. J. Ashok, Y. Kathiraser, M. L. Ang, S. Kawi, Bi-functional hydrotalcite-derived NiO–CaO–Al_2O_3 catalysts for steam reforming of biomass and/or tar model compound at low steam-to-carbon conditions. *Appl. Catal. B* **172–173**, 116–128 (2015).
22. M. Romero, A. Steinfeld, Concentrating solar thermal power and thermochemical fuels. *Energy Environ. Sci.* **5**, 9234–9245 (2012).
23. D. Marxer, P. Furler, M. Takacs, A. Steinfeld, Solar thermochemical splitting of CO_2 into separate streams of CO and O_2 with high selectivity, stability, conversion, and efficiency. *Energy Environ. Sci.* **10**, 1142–1149 (2017).
24. J. Wang, L. Huang, R. Yang, Z. Zhang, J. Wu, Y. Gao, Q. Wang, D. O'Hare, Z. Zhong, Recent advances in solid sorbents for CO_2 capture and new development trends. *Energy Environ. Sci.* **7**, 3478–3518 (2014).
25. E. S. Sanz-Pérez, C. R. Murdock, S. A. Didas, C. W. Jones, Direct capture of CO_2 from ambient air. *Chem. Rev.* **116**, 11840–11876 (2016).
26. K. Li, B. Peng, T. Peng, Recent advances in heterogeneous photocatalytic CO_2 conversion to solar fuels. *ACS Catal.* **6**, 7485–7527 (2016).
27. F. Li, D. R. MacFarlane, J. Zhang, Recent advances in the nanoengineering of electrocatalysts for CO_2 reduction. *Nanoscale* **10**, 6235–6260 (2018).
28. J. Wu, Y. Huang, W. Ye, Y. Li, CO_2 reduction: From the electrochemical to photochemical approach. *Adv. Sci.* **4**, 1700194 (2017).
29. F. A. Rahman, M. M. A. Aziz, R. Saidur, W. A. W. A. Bakar, M. R. Hainin, R. Putrajaya, N. A. Hassan, Pollution to solution: Capture and sequestration of carbon dioxide (CO_2) and its utilization as a renewable energy source for a sustainable future. *Renew. Sust. Energ. Rev.* **71**, 112–126 (2017).
30. C. A. Trickett, A. Helal, B. A. Al-Maythalony, Z. H. Yamani, K. E. Cordova, O. M. Yaghi, The chemistry of metal-organic frameworks for CO_2 capture, regeneration and conversion. *Nat. Rev. Mater.* **2**, 17045 (2017).
31. R. K. Singha, A. Yadav, A. Agrawal, A. Shukla, S. Adak, T. Sasaki, R. Bal, Synthesis of highly coke resistant Ni nanoparticles supported MgO/ZnO catalyst for reforming of methane with carbon dioxide. *Appl. Catal. B* **191**, 165–178 (2016).
32. M. Peymani, S. M. Alavi, M. Rezaei, Synthesis gas production by catalytic partial oxidation of methane, ethane and propane on mesoporous nanocrystalline Ni/Al_2O_3 catalysts. *Int. J. Hydrogen Energy* **41**, 19057–19069 (2016).
33. X. Chen, J. Jiang, S. Tian, K. Li, Biogas dry reforming for syngas production: Catalytic performance of nickel supported on waste-derived SiO_2. *Catal. Sci. Technol.* **5**, 860–868 (2015).
34. R. K. Singha, A. Yadav, A. Shukla, Z. Iqbal, C. Pendem, K. Sivakumar, R. Bal, Promoting effect of CeO_2 and MgO for CO_2 reforming of methane over Ni-ZnO catalyst. *ChemistrySelect* **1**, 3075–3085 (2016).
35. B. Jiang, L. Li, Z. Bian, Z. Li, Y. Sun, Z. Sun, D. Tang, S. Kawi, B. Dou, M. A. Goula, Chemical looping glycerol reforming for hydrogen production by Ni@ZrO_2 nanocomposite oxygen carriers. *Int. J. Hydrogen Energy* **43**, 13200–13211 (2018).
36. B. Jiang, L. Li, Z. Bian, Z. Li, M. Othman, Z. Sun, D. Tang, S. Kawi, B. Dou, Hydrogen generation from chemical looping reforming of glycerol by Ce-doped nickel phyllosilicate nanotube oxygen carriers. *Fuel* **222**, 185–192 (2018).
37. J. Zhang, F. Li, Coke-resistant Ni@SiO_2 catalyst for dry reforming of methane. *Appl. Catal. B* **176–177**, 513–521 (2015).
38. R. C. Rabelo-Neto, H. B. E. Sales, C. V. M. Inocêncio, E. Varga, A. Oszko, A. Erdohelyi, F. B. Noronha, L. V. Mattos, CO_2 reforming of methane over supported $LaNiO_3$ perovskite-type oxides. *Appl. Catal. B* **221**, 349–361 (2018).
39. G. A. Olah, A. Goeppert, M. Czaun, G. K. Surya Prakash, Bi-reforming of methane from any source with steam and carbon dioxide exclusively to metgas ($CO–2H_2$) for methanol and hydrocarbon synthesis. *J. Am. Chem. Soc.* **135**, 648–650 (2013).
40. Y. Zheng, K. Li, H. Wang, D. Tian, Y. Wang, X. Zhu, Y. Wei, M. Zheng, Y. Luo, Designed oxygen carriers from macroporous $LaFeO_3$ supported CeO_2 for chemical-looping reforming of methane. *Appl. Catal. B* **202**, 51–63 (2017).
41. Q. Jing, H. Lou, L. Mo, X. Zheng, Comparative study between fluidized bed and fixed bed reactors in methane reforming with CO_2 and O_2 to produce syngas. *Energy Convers. Manag.* **47**, 459–469 (2006).
42. F. Gallucci, M. Van Sintannaland, J. A. M. Kuipers, Theoretical comparison of packed bed and fluidized bed membrane reactors for methane reforming. *Int. J. Hydrogen Energy* **35**, 7142–7150 (2010).
43. M. Tang, L. Xu, M. Fan, Progress in oxygen carrier development of methane-based chemical-looping reforming: A review. *Appl. Energy* **151**, 143–156 (2015).
44. C.-j. Liu, J. Ye, J. Jiang, Y. Pan, Progresses in the preparation of coke resistant Ni-based catalyst for steam and CO_2 reforming of methane. *ChemCatChem* **3**, 529–541 (2011).
45. T. V. Choudhary, V. R. Choudhary, Energy-efficient syngas production through catalytic oxy-methane reforming reactions. *Angew. Chem. Int. Ed.* **47**, 1828–1847 (2008).
46. R. C. Maher, V. Duboviks, G. J. Offer, M. Kishimoto, N. P. Brandon, L. F. Cohen, Raman spectroscopy of solid oxide fuel cells: Technique overview and application to carbon deposition analysis. *Fuel Cells* **13**, 455–469 (2013).
47. Z. Li, S. Das, P. Hongmanorom, N. Dewangan, M. H. Wai, S. Kawi, Silica-based micro- and mesoporous catalysts for dry reforming of methane. *Catal. Sci. Technol.* **8**, 2763–2778 (2018).
48. Z. Bian, S. Das, M. H. Wai, P. Hongmanorom, S. Kawi, A review on bimetallic nickel-based catalysts for CO_2 reforming of methane. *ChemPhysChem* **18**, 3117–3134 (2017).
49. A. M. Kierzkowska, R. Pacciani, C. R. Müller, CaO-based CO_2 sorbents: From fundamentals to the development of new, highly effective materials. *ChemSusChem* **6**, 1130–1148 (2013).
50. M. P. Pechini, Method of preparing lead and alkaline earth titanates and niobates and coating method using the same to form a capacitor. U.S. Patent 3330697 (1967).
51. M. Kakihana, M. Yoshimura, Synthesis and characteristics of complex multicomponent oxides prepared by polymer complex method. *Bull. Chem. Soc. Jpn.* **72**, 1427–1443 (1999).
52. R. W. Cheary, A. Coelho, A fundamental parameters approach to X-ray line-profile fitting. *J. Appl. Cryst.* **25**, 109–121 (1992).
53. A. V. Naumkin, A. Kraut-Vass, S. W. Gaarenstroom, C. J. Powell, NIST X-ray Photoelectron Spectroscopy Database; https://srdata.nist.gov/xps/.

Acknowledgments: We thank Y. Jiang and K. Imrie from Macquarie University for providing sponsorship for this research and proofreading the manuscript, respectively. We thank Y. Zhu from Macquarie University and G. Li from Shanghai University for help with XRD analysis. We thank X. Yang from Macquarie University for help with material preparation. **Funding:** We acknowledge the financial support from the 2017 Macquarie University Research Fellowship (MQRF) Scheme for S.T. We would also like to acknowledge the National Natural Science Foundation of China (grant no. 21776160) and the National Natural Science Fund for Outstanding Young Scholars of China (grant no. 51522401). **Author contributions:** S.T. conceived the study and developed the sorbent-catalysts. S.T. and F.Y. performed the material characterization. S.T. and J.J. performed process tests and thermodynamic calculations. S.T. and Z.Z. conducted the analysis. S.T. wrote the paper. All authors discussed the results and commented on the manuscript. **Competing interests:** The authors declare that they have no competing interests. **Data and materials availability:** All data needed to evaluate the conclusions in the paper are present in the paper and/or the Supplementary Materials. Additional data related to this paper may be requested from the authors.

Submitted 23 September 2018
Accepted 19 February 2019
Published 12 April 2019
10.1126/sciadv.aav5077

Citation: S. Tian, F. Yan, Z. Zhang, J. Jiang, Calcium-looping reforming of methane realizes in situ CO_2 utilization with improved energy efficiency. *Sci. Adv.* **5**, eaav5077 (2019).

Science Advances

Calcium-looping reforming of methane realizes in situ CO_2 utilization with improved energy efficiency

Sicong Tian, Feng Yan, Zuotai Zhang and Jianguo Jiang

Sci Adv **5** (4), eaav5077.
DOI: 10.1126/sciadv.aav5077